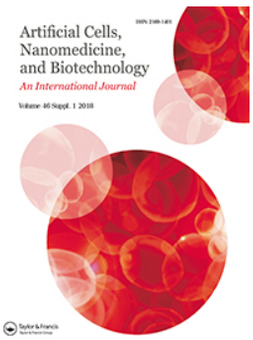

Taylor & Francis
Taylor & Francis Group

Artificial Cells, Nanomedicine, and Biotechnology
An International Journal

ISSN: 2169-1401 (Print) 2169-141X (Online) Journal homepage: https://www.tandfonline.com/loi/ianb20

Selective heat generation in cancer cells using a combination of 808 nm laser irradiation and the folate-conjugated Fe_2O_3@Au nanocomplex

Mehri Mirrahimi, Vahid Hosseini, S. Kamran Kamrava, Neda Attaran, Jaber Beik, Siavash Kooranifar, Habib Ghaznavi & Ali Shakeri-Zadeh

To cite this article: Mehri Mirrahimi, Vahid Hosseini, S. Kamran Kamrava, Neda Attaran, Jaber Beik, Siavash Kooranifar, Habib Ghaznavi & Ali Shakeri-Zadeh (2018) Selective heat generation in cancer cells using a combination of 808 nm laser irradiation and the folate-conjugated Fe_2O_3@Au nanocomplex, Artificial Cells, Nanomedicine, and Biotechnology, 46:sup1, 241-253, DOI: 10.1080/21691401.2017.1420072

To link to this article: https://doi.org/10.1080/21691401.2017.1420072

ARTIFICIAL CELLS, NANOMEDICINE, AND BIOTECHNOLOGY
2018, VOL. 46, NO. S1, S241–S253
https://doi.org/10.1080/21691401.2017.1420072

Selective heat generation in cancer cells using a combination of 808 nm laser irradiation and the folate-conjugated Fe_2O_3@Au nanocomplex

Mehri Mirrahimi[a,b], Vahid Hosseini[a,b], S. Kamran Kamrava[c,d], Neda Attaran[c], Jaber Beik[a,b], Siavash Kooranifar[e], Habib Ghaznavi[f] and Ali Shakeri-Zadeh[a,b]

[a]Radiation Biology Research Center, Iran University of Medical Sciences, Tehran, Iran; [b]Medical Physics Department, School of Medicine, Iran University of Medical Sciences (IUMS), Tehran, Iran; [c]Applied Biophotonics Research Center, Science and Research Branch, Islamic Azad University, Tehran, Iran; [d]ENT and Head & Neck Research Center and Department, Iran University of Medical Sciences (IUMS), Tehran, Iran; [e]Department of Pulmonary Medicine, Hazrat Rasoul Akram Hospital, Iran University of Medical Sciences (IUMS), Tehran, Iran; [f]Cellular and Molecular Research Center, Zahedan University of Medical Sciences (ZaUMS), Zahedan, Iran

ABSTRACT

Photothermal therapy (PTT) is a nanotechnology-assisted cancer hyperthermia approach in which the interaction between laser light and plasmonic nanoparticles (NPs) generates localized heating. The exploitation of plasmonic NPs in association with active targeting moieties causes the preferential accumulation of NPs inside cancer cells, thereby providing targeted PTT. Herein, we evaluate the effect of folic acid (FA) as an active targeting agent in enhancing the photothermal efficiency of multifunctional Iron (III) Oxide (Fe_2O_3)@Au core- shell NPs. Fe_2O_3@Au NPs were synthesized, modified with FA and then characterized. Human nasopharyngeal (KB) cancer cells were treated with different concentrations of Fe_2O_3@Au, with and without FA modification and the temperature rise profiles of the cells were measured upon administration of the near-infrared (NIR) laser (808 nm, 6 W/cm^2, 10 min). The recorded temperature profiles of the cells were used for thermal dose calculation. Finally, the level of induced apoptosis was determined by flow cytometry using an annexin V-fluorescein isothiocyanate/propidium iodide apoptosis detection kit. The characterization data showed that the Fe_2O_3@Au NPs are spherical, with a hydrodynamic size of 33 nm. The data corroborated the successful conjugation of the NPs with FA. The thermometry results indicated the superior temperature elevation rate of the cells in the presence of the NPs upon NIR irradiation. Meanwhile, the higher heating rate and the higher thermal dose were obtained for the cells exposed to FA-targeted Fe_2O_3@Au rather than the non-targeted nanocomplex. Flow cytometry studies revealed that FA-targeted Fe_2O_3@Au induced higher level of apoptosis than non-targeted Fe_2O_3@Au NPs. In conclusion, our findings suggest that the synthesized FA-targeted Fe_2O_3@Au NP has high potentials to be considered as an efficient thermosensitizer in the process of targeted cancer hyperthermia.

ARTICLE HISTORY
Received 19 September 2017
Revised 12 December 2017
Accepted 18 December 2017

KEYWORDS
Nanotechnology; hyperthermia; folic acid; cancer targeting; thermal dose; apoptosis

Introduction

In spite of the extensive progress made in the area of cancer therapy, this disease is still the second-leading cause of mortality worldwide. Recent efforts in this area have focused on the implementation of nanotechnology to improve the current efficiency of cancer diagnosis and therapy. The use of nanoprobes in association with biomedical imaging has exhibited great promise in eliminating the current detection limits of cancer diagnosis [1,2]. On the other hand, chemotherapy and radiotherapy, are the major lines of cancer therapy, have been subjected to considerable improvements through incorporation with nanomaterials [3–7].

Hyperthermia is thought to be another important action domain in the area of cancer therapy. Cancer hyperthermia subscribes to the strategy of elevating the temperature of the tumor, which either induces the immediate killing of cancer cells if the temperature is high enough (>45 °C) or renders the cancer cells more vulnerable to various therapeutic modalities for smaller increases in temperature (40–45 °C) [8,9]. Many clinical experiments have reported improved local tumor control and overall survival in cancer patients by the implementation of hyperthermia as an adjuvant therapy in association with chemotherapy or radiotherapy [10,11].

As the hyperthermia energy source propagates throughout the patient body, the tumor and its collateral healthy tissue indiscriminately undergo temperature elevation, resulting in unwanted thermal damages. In nanotechnology-assisted hyperthermia, however, the tumors are impregnated with the suitable nanoparticles (NPs) that are able to absorb the energy of the hyperthermia source and induce localized heating [12]. This strategy confines the thermal damage to the tumor site only and keeps the collateral tissues safe [13].

Photothermal therapy (PTT) is considered a beneficial nanotechnology-assisted hyperthermia approach in which plasmonic NPs are subjected to laser light in order to absorb

CONTACT Habib Ghaznavi ghaznavih@yahoo.com Cellular and Molecular Research Center, Zahedan University of Medical Sciences (ZaUMS), Zahedan, Iran; Ali Shakeri-Zadeh shakeriz@iums.ac.ir Iran University of Medical Sciences (IUMS), Hemmat Exp., Tehran, Iran

optical energy and turn it into heat, thus providing a localized hyperthermia strategy. Compared to magnetic hyperthermia, the most established nanotechnology-assisted hyperthermia method, where magnetic NPs generate heat under an alternating magnetic field, PTT benefits from much greater heat generation efficiency, making it an attractive area for research [14–16].

Among all the plasmonic NPs identified to date, gold NPs (AuNPs) have been introduced as elegant light-responsive nanomaterials due to their (i) ideal thermophysical properties, (ii) suitable size for passive accumulation inside the tumor, (iii) synthetic versatility for fine-tuning size and morphology, (iv) conjugation with active targeting ligands and (v) inclusion in biomedical imaging [17–20].

A key perquisite for tumor-specific PTT while preserving surrounding healthy tissue is to accurately direct AuNPs towards cancer cells [21–23]. This may be provided by the exploitation of the active targeting strategy that is based on the specific identification of targeting ligands (e.g. proteins, peptides, aptamers and small molecules) conjugated to AuNPs by cancer cell surface receptors [23]. The vitamin folic acid (FA) is a necessary ingredient for cell proliferation. Due to their rapid division rate cancerous cells generally indicate a higher level of FA receptor expression on their surface than normal cells in order to meet this need. FA modification of AuNPs thus endows the NPs with a unique capability to particularly target cancer cells [24–27].

Besides the use of multimodal imaging modalities, the real-time guidance of PTT operation is an interesting success in this area that can further promote the safety and the efficiency of PTT. For example, the unique properties of magnetic NPs in the magnetic resonance imaging (MRI) contrast agent in addition to the light-absorbing properties of AuNPs have recently led to the development of a multifunctional magneto-plasmonic nanoplatform, providing the capability of MRI-guided PTT [28].

This study aims to demonstrate the heat generation capability of the Iron (III) Oxide (Fe_2O_3)@Au nanocomplex on illumination by the NIR laser. To this end, the direct temperature rise of KB cancer cells loaded with the NPs was monitored during the PTT operation. For illustrating the role of FA targeting on improving the efficiency of PTT, the temperature rise of cancer cells loaded with FA-modified Fe_2O_3@Au nanocomplex (Fe_2O_3@Au-FA) was further evaluated. In addition, for a better understanding of how the FA-targeting strategy is efficient in promoting the PTT regimes in the clinic, the thermometry results were analyzed based on the practical parameters of the thermal dose. Finally, we determined and compared the level of cancer cell apoptosis when FA-targeted or non-targeted Fe_2O_3@Au NP is used in the process of PTT.

Materials and methods

Material

Iron (II) chloride tetrahydrate (> 99%), iron (III) chloride hexahydrate (> 99%), ammonia (32%), hydrochloric acid (HCl), Nitric acid (HNO_3), N-hydroxysuccinimide, dicyclohexylcarbodiimide and cysteamine were purchased from Merck (Darmstadt, Germany). Fetal bovin serum (FBS) was purchased from BioSera Ltd. (Ringmer, United Kingdom). Dubelco's Modification of Eagle's Medium (DMEM) was purchased from GIBCO (Invitrogen, Germany). Trypsin- ethylene diamine tetra acetic acid (EDTA), dimethyl sulfoxide (DMSO), penicillin-streptomycin solution, folic acid and Gold (III) chloride solution, all were purchased from Sigma-Aldrich Corp. (St Louis, MO).

Synthesis of Fe_2O_3@Au core-shell NPs

Fe_2O_3@Au core-shell NPs were prepared through the oxidation of Ferroferric oxide (Fe_3O_4) NPs in the aqueous phase [29]. Briefly, 2.6 g of ferric chloride and 1.0 gr of ferrous chloride were dissolved in HCl solution (12 M) and 12.5 ml of water. The solution was introduced into sodium hydroxide solution through dropwise addition (125.0 ml, 1.5 M) with vigorous stirring. The generated black precipitate was collected using a magnet and the supernatant was removed from the precipitate through decantation. After washing the precipitate for three times using 50 ml of water, HCl solution (250 ml, 0.01 M) was added to neutralize the anionic charges of the precipitate; the resulting Fe_3O_4 NPs were obtained after washing with water. The freshly prepared Fe_3O_4 NPs were further dissolved in HNO_3 (0.01 M) and heated under stirring at 100 °C for one hour in order to completely oxidize the Fe_3O_4 NPs to Fe_2O_3 NPs. The solution was then cooled to room temperature and washed twice using water, followed by centrifugation at 10,000 RPM for 15 min. Fe_2O_3@Au core-shell NPs were synthesized through the deposition of Au on Fe_2O_3 NPs using the modified Lyon's iterative hydroxylamine-seeding procedure [30]. First, Fe_2O_3 NPs (1.0 ml, 1.1 mM) was mixed with sodium citrate (1.0 ml, 0.1 M) for 10 min, followed by dilution with 20 ml H_2O. Subsequently, 0.1 ml of hydroxylamine hydrochloride ($NH_2OH{\cdot}HCl$) solution and 1.0 ml of Chloroauric acid ($HAuCl_4$) solution were added dropwise under stirring for a total of 50 min. The addition of $NH_2OH{\cdot}HCl$ and $HAuCl_4$ was repeated twice. The solution changed to garnet after three iterative additions.

Preparation of cysteamine-FA conjugate

First, as shown in Scheme 1(a), the FA N-hydroxysuccinimide (FA-NHS) active ester was synthesized using a previously reported method with a minor modification [31,32]. A solution of anhydrous DMSO and triethylamine (100:1) was stirred for 10 min. Then 0.25 g of FA was added gradually to the above mixture which was continuously stirred in the dark, and kept overnight. Later FA was mixed with 0.1 g of dicyclohexylcarbodiamide and 0.1 g of N-hydroxysuccinimide and was stirred for another 24 h. The by-product, dicyclohexylurea (DCU), was removed by filtration. DMSO and triethylamine were evaporated under vacuum. Second, for the preparation of the cysteamine-FA conjugate, vacuum-dried FA-NHS was dissolved in the mixture of DMSO and trimethylamine (2:1). Later, 0.1 g cysteamine was added to the mixture and stirred overnight. The resulting yellow solid (cysteamine-FA

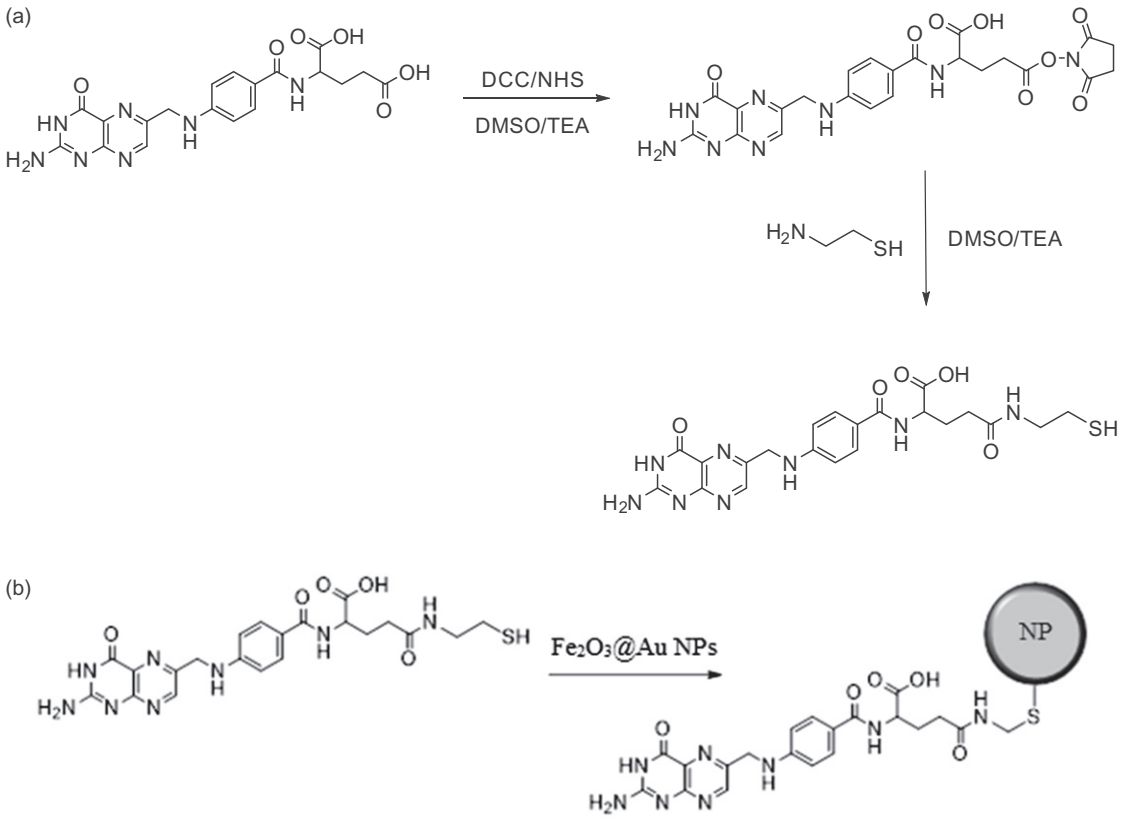

Scheme 1. (a) Preparation of cysteamine-folic acid conjugate. DCC: dicyclohexylcarbodiimide;NHS: N-hydroxysuccinimide; DMSO: dimethyl sulfoxide; TEA trimethylamine. (b) Surface modification of Fe_2O_3@Au core-shell nanoparticles with cysteamine-folic acid conjugate.

conjugate) was obtained by filtration and was washed with ethyl ether twice.

Surface modification of Fe_2O_3@Au core-shell NPs with the cysteamine-FA conjugate

Conjugation of cysteamine-FA on the Fe_2O_3@Au surface involved the following method [33]: The dried cysteamine-FA conjugate was added gradually to the solution of prepared Fe_2O_3@Au and the mixture was stirred for four hours at room temperature to form cysteamine-FA conjugated gold NPs (Scheme 1(b)). Finally, the prepared cysteamine-FA conjugated Fe_2O_3@Au core-shell NPs were purified by centrifugation and double re-precipitation from distilled water.

Nanoparticle characterization

The morphology and size distribution of the synthesized NPs were analyzed by high-resolution transmission electron microscopy (HR-TEM). The hydrodynamic diameter of the NPs and their surface charge were measured by dynamic light scattering (DLS), using the Malvern Zetasizer Nano ZS-90 instrument. The UV-Visible (UV-Vis) absorption spectra of the NPs dispersed in water were recorded using the Rayleigh UV-1601 instrument. Fourier transform infra-red (FTIR) spectra were recorded using the Shimadzu FT-IR 4300 instrument equipped with pressed potassium bromide pellets at room temperature. FTIR studies were considered in order to confirm the surface functionalization of the nanoconjugate. The magnetic properties of the nanocomplex were determined using a vibrating sample magnetometer (VSM; MDK6, Kavir, Iran).

Cell culture

Cell culture was accomplished in accordance with institutional guidelines with permission received from Ethic Committee of Iran University of Medical Sciences (IUMS) under the code of "IR.IUMS.REC 1395.95–04-223–9411338004". Our experiments were conducted on the KB cell line, derived from human mouth epidermal carcinoma. The cells were cultured as a monolayer in the DMEM cell growth media with L-glutamine and sodium hydroxide supplemented with 10% FBS, 100 units/ml penicillin and 100 μg/ml streptomycin was incubated in a humidified atmosphere containing 5% CO_2 and 95% air at 37 °C.

In vitro experimental procedure

To perform the PTT operation, the KB cells were seeded in a 96-well cell culture plate at a density of 1×10^4 cells per well and incubated for 24 h at 37 °C in a humidified 5% CO_2 atmosphere. The medium solution containing the Fe_2O_3@Au and the Fe_2O_3@Au-FA nanocomplex with different Au concentrations of 20, 30 and 40 μg/ml were prepared and added to the cells. After incubation for another four hours, the culture medium was removed. The cells were washed twice with PBS to remove the unloaded NPs and later fresh medium was added. In order to initiate the PTT operation from the normal body temperature, the culture plate was

placed on a warm surface at a constant temperature of 37 °C. After reaching thermal equilibrium between the surface and the culture plate, the cells were irradiated by a continuous-wave 808 nm laser source (Nanobon Company, Tehran, Iran) at an intensity of 6 W/cm^2 for 10 min. To observe the photothermal heating efficiency of Fe_2O_3@Au and the Fe_2O_3@Au-FA nanocomplex, the transient temperature variations of the cells were monitored with an infrared (IR) thermal camera (Testo 875–1i, Germany) during the laser irradiation process.

Thermal dose calculations

The thermal dose was calculated using the corresponding time-temperature profile of the cells according to the method developed by Separeto and Dewey, in which the thermal dose parameter was expressed as CEM 43 °C and was calculated using Equation (1):

$$\text{CEM } 43^{\circ}\text{C} = \int_0^t R_{CEM}{}^{(43-T)}\,dt \quad (1)$$

where t is the time spent at temperature T and R_{CEM} is the ratio of exposure times that result in the same cell survival for a 1 °C rise in temperature. For many cell types, R_{CEM} is generally considered to be 0.5 for temperatures above 43 °C and 0.25 for temperatures below 43 °C [34,35].

3-(4,5-dimethylthiazol-2-yl)-2,5-diphenyltetrazolium bromide (MTT) assay

To test the cytotoxicity of core-shell nanocomplex, the viability of KB cells incubated by various concentration of the nanocomplex was evaluated using MTT tetrazolium assay, which measures the ability of metabolically active mitochondria in live cells to reduce a colorless tetrazolium compound to a blue formazan product. To perform this assay, cells were incubated with various concentrations of nanocomplex (10, 15, 20, 30 and 40 μg/ml). After four hours, the nanocomplex was removed and cells were washed with PBS. After adding 100 μl of FBS-free culture medium, 10 μl MTT dye (at a concentration of 5 mg/ml) was also added to each well and the plate was incubated for four hours. Then, MTT-containing medium was removed and was replaced with DMSO (10 μl per well) to dissolve the formazan crystals which was kept in the dark at room temperature for 15 min. Later the absorbance of the dissolved formazan was read at wavelength of 570 nm by an ELISA reader (DYNEX MRX, USA) using a reference wavelength of 630 nm. The relative survival of KB cells was represented as the absorbance of the treated sample/absorbance of the control group. The optical density (OD) of dissolved formazan is directly proportional to living cells. In our experiments, we designed control groups beside the treated groups and therefore, the cell viability percentage was calculated using Equation (2):

$$\text{Cell viability } (\%) = \frac{(\text{OD}_{\text{sample}} - \text{OD}_{\text{medium}})}{(\text{OD}_{\text{control}} - \text{OD}_{\text{medium}})} \times 100 \quad (2)$$

In addition, cytotoxicity tests were similarly repeated for FA-conjugated nanocomplex, but only at concentration of 20 μg/ml, because this concentration was selected for PTT experiments.

All experiments were repeated at least three times.

Flow cytometry

The extent of apoptosis was measured through annexin V-fluorescein isothiocyanate (FITC) apoptosis detection kit as described in the manufacturer's instructions (eBioscience, San Diego, CA). After performing PTT experiments on the KB cells [(laser parameters: 808 nm; 6 W/cm^2; 10 min) and (incubation conditions: 20 μg/ml for 4 h)], the cells were plated at a density of 200,000 cells/well in flat bottom 24-well plates. In brief, cells were harvested and centrifuged at 300 g for 5 min. Then cells were washed once with PBS) and once with 1 × binding buffer. After that, cells were suspended in 1 × binding buffer and 5 μl of flurochrome-conjugated annexin V was added to 100 μl of cell suspension and incubated for 15 min in dark at room temperature. Cells were then washed once again with 2 ml of binding buffer and was suspended in 200 μl of 1 × binding buffer. Finally, 5 μl of propidum iodide (PI) staining solution was added to 200 μl cell suspensions and assessed by flow cytometer (BD FACSCantoII, BD Biosciences, Franklin Lakes, NJ).

Statistical analysis

Statistical analysis was performed by using the SPSS software (SPSS, Chicago, IL,version 11). The one-way analysis of variance (ANOVA) statistical method was used to evaluate the significance of the experimental data. A value of $p < .05$ was considered statistically significant.

Results

Nanoparticle characterization

Figure 1 shows the TEM images of targeted and non-targeted Fe_2O_3@Au core–shell NPs in which the Au shell could be obviously seen on the surface of Fe_2O_3 NPs. As shown in Figure 1(a), the magnetic core of the prepared Fe_2O_3@Au nanocomplex is ~20 nm thick and the gold layer was <3 nm thick. According to Figure 1(c), the hydrodynamic diameter of the NPs measured by DLS analysis ranged between 20 and 50 nm, with the highest frequency of 33 nm. Figure 1(d) shows size distribution of FA functionalized Fe_2O_3@Au nanocomplex in which hydrodynamic diameter of the NPs ranged from 30 to 70 nm, with the highest frequency of 46 nm.

The zeta potential of the Fe_2O_3@Au nanocomplex was −17.9 mV, whereas after FA modification, the zeta potential was changed to −22.4 mV (Figure 2). UV-Vis spectrometry was utilized to characterize the synthesized Fe_2O_3@Au-FA core-shell NPs (Figure 3). It is clear that the Fe_2O_3@Au-FA core-shell NPs display a typical surface plasmon broadened band at 606 nm, indicative of the formation of Fe_2O_3@Au-FA core-shell NPs, whereas the Fe_2O_3@Au core-shell NPs display characteristic surface plasmon absorption at 584 nm.

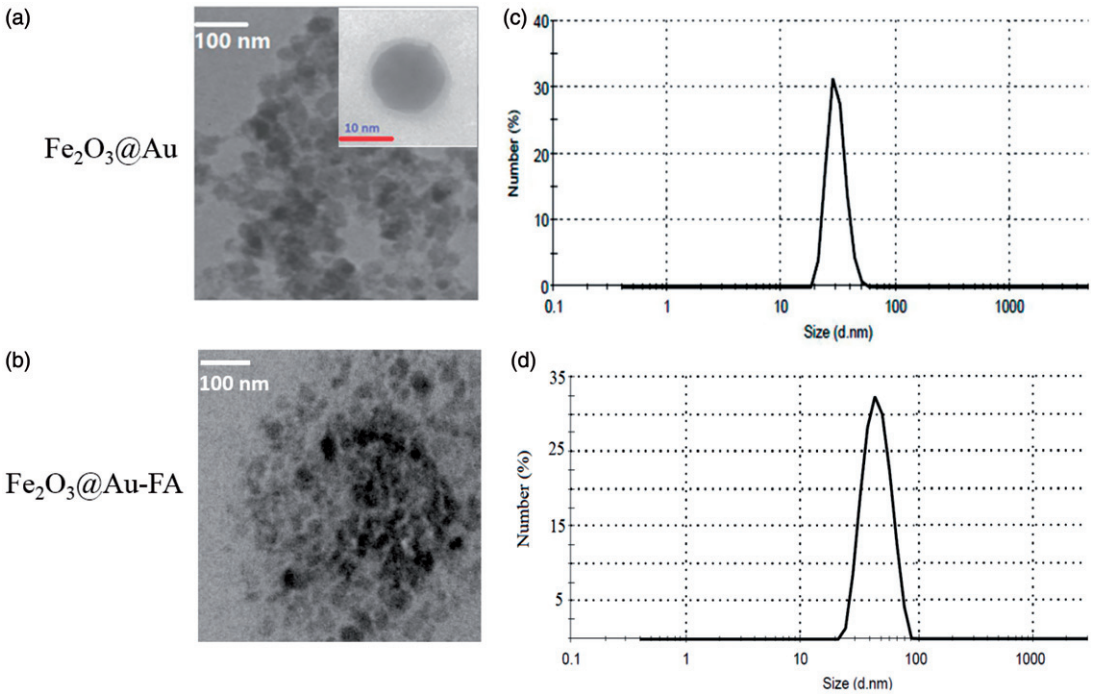

Figure 1. TEM images(a,b) and DLS of the synthesized core-shell nanoparticles (with and without FA; (c,d)).

This red-shift in the position of the maximum absorption indicates that FA has interacted with the Fe_2O_3@Au core-shell NPs. In addition, the absorption peak at 304 nm is likely to be ascribed to the attached FA moieties [36]. As a consequence, the change in color of the Fe_2O_3@Au-FA core-shell NPs occur (Figure 3(c)). The reason behind this alteration in color may be due to the change in particle size and the alteration in the refractive index of the medium or in the peripheral region of the particle [37].

The conjugation of the folate to Fe_2O_3@Au was verified by comparing the FTIR spectra of FA and Fe_2O_3@Au-cysteamine-FA (Figure 4(a,b)). The band at 1315 cm^{-1} corresponds to the asymmetric stretching vibration of $-NH_2$ in the folate; the bands at 1627 and 1677 cm^{-1} relate to the C = O stretching in carboxyl acids; the band at 1516 cm^{-1} belongs to the C = O bond stretching vibration of the –CONH– group; the bands between 3000 and 3500 cm^{-1} are due to the O–H stretching and NH-stretching vibration bands of FA and cysteamine [38]. In addition, the absence of the absorption band at 2100–2300 cm^{-1} is attributed to the characteristic absorption of -SH of cysteamine by the surface of the AuNPs, suggesting that –SH conjugated with Au on the surface of the NPs. The bands at 2850–2927 cm^{-1} relate to the asymmetric and symmetric C-H stretching vibrations of $-CH_2$.

The magnetic properties of Fe_2O_3@Au nanocomplex and Fe_2O_3@Au-FA nanoconjugate were determined using VSM. As seen in Figure 5, for the synthesized nanocomplexes, no hysteresis was detected.

Thermometry results

Temperature monitoring of the cells loaded with NPs during the PTT operation demonstrated that the Fe_2O_3@Au NPs possess a strong light-absorption capability. While KB cells without NPs showed a negligible temperature rise on laser irradiation, the presence of Fe_2O_3@Au NPs inside the cells appreciably increased the cell temperature. In addition, such temperature enhancement seems to vary with the concentration of NPs. Following NIR laser irradiation, KB cells treated with higher concentrations of NPs reached higher temperatures. The temperature rise profiles of the cells incubated with different concentrations of Fe_2O_3@Au and Fe_2O_3@Au-FA and irradiated by 808 nm laser are shown in Figures 5 and 6, respectively. After 10 min of laser irradiation, the temperature of the cells increased from 37 °C to 37.7 ± 0.3 °C, whereas the temperature significantly increased to 40.2 ± 0.35 °C, 41.2 ± 0.4 °C and 42.9 ± 0.3 °C for those cells that were exposed to Fe_2O_3@Au with different Au concentrations of 20, 30, and 40 μg/ml, respectively (Figure 7). Expressing similar behavior, the temperature of the cells exposed to Fe_2O_3@Au-FA NPs raised to 43.9 ± 0.6 °C, 45.9 ± 0.6 °C, and 48.5 ± 0.5 °C demonstrated the superior heat-generation capability of Fe_2O_3@Au-FA over Fe_2O_3@Au (Figure 7). It should be noted that the photothermal conversion inherent capability of Fe_2O_3@Au does not vary when functionalized with FA. In the case of Fe_2O_3@Au conjugated with FA, intracellular accumulation of the NPs via receptor-mediated endocytosis is enhanced. Accordingly, KB cells treated with Fe_2O_3@Au-FA are expected to have higher intracellular Au content than the cells treated with non-targeted NPs at the same concentration. Consequently, upon NIR irradiation, the cells with higher Au content show a higher temperature elevation than those cells treated with non-targeted NPs.

Figure 8 shows a comparison between the final temperature increase of the cells exposed to Fe_2O_3@Au and Fe_2O_3@Au-FA, with different concentrations at the end of 10 min of irradiation with the NIR laser. Compared to non-

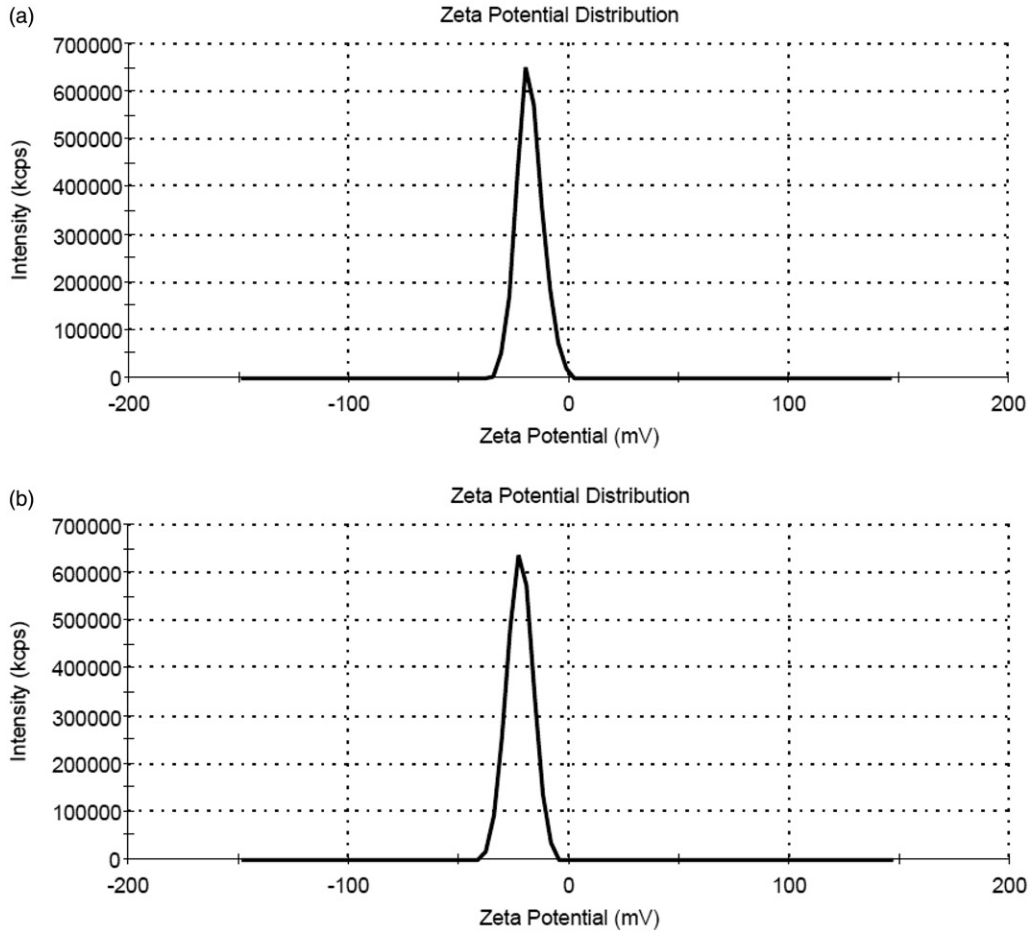

Figure 2. Surface charge distribution of (a) Fe_2O_3@Au and (b) Fe_2O_3@Au-FA nanocomplex by zeta potential measurement.

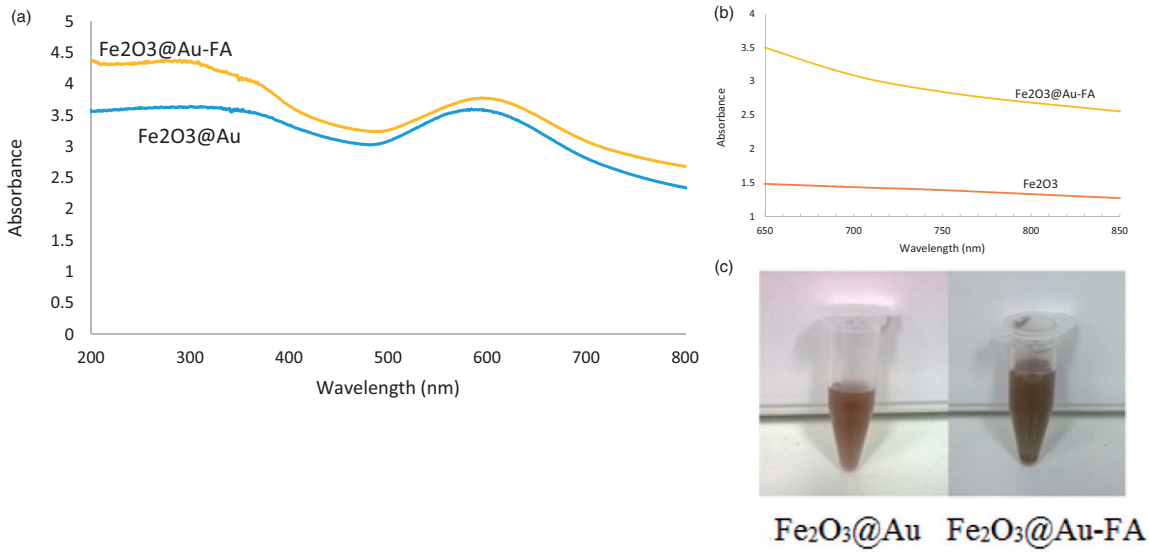

Figure 3. (a) UV-Vis spectra show a red-shift in the surface plasmon resonance of Fe_2O_3@Au core-shellNPs due to attachment to the FA-cysteamine. (b) UV-Vis spectra of FA conjugated Fe_2O_3@Au core shell NPs and Fe_2O_3 NPs in water. Arrow shows the wavelength of the laser utilized for PTT. (c) Change in the color of colloidal Fe_2O_3@Au core-shell NPs from garnet (left) to grayish brown (right) after formation of the FA conjugated Fe_2O_3@Au complex.

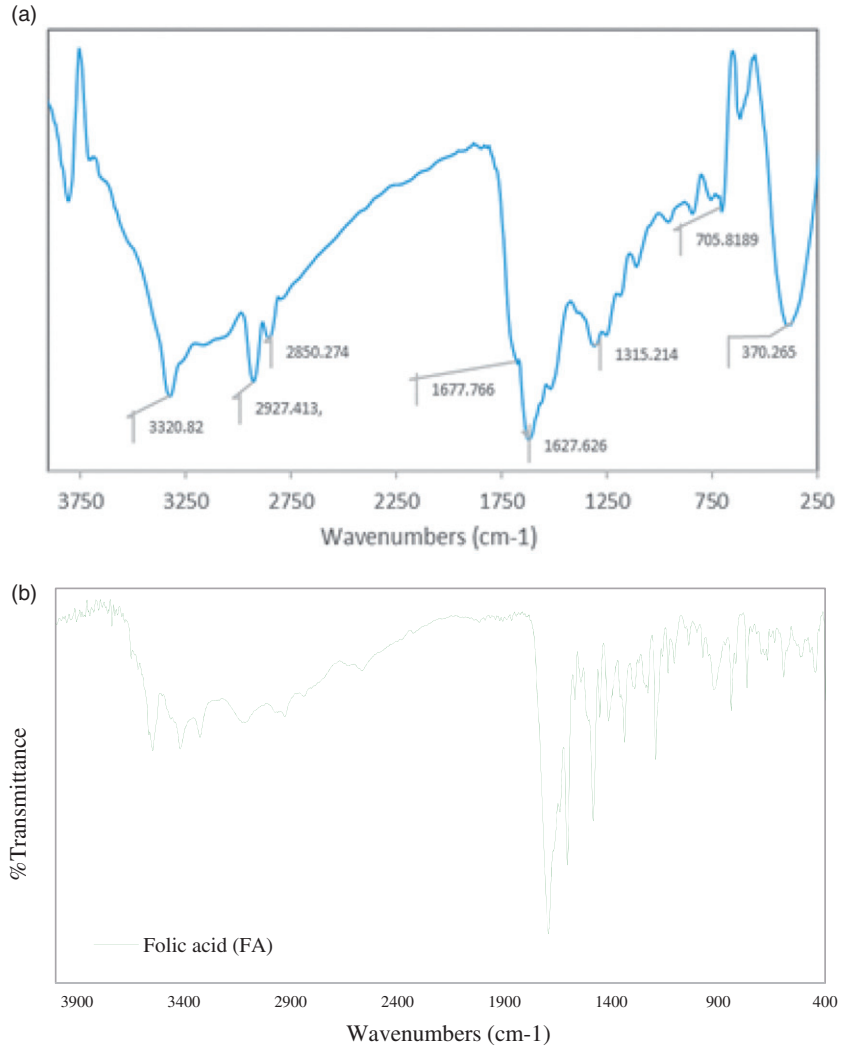

Figure 4. Fourier transform infrared (FTIR) spectra of (a) Fe_2O_3@Au-cysteamine-FA nanoconjugate and (b) FA.

targeted Fe_2O_3@Au, the cells exposed to the Fe_2O_3@Au-FA indicated a higher temperature increase.

Thermal dose

To estimate the effects of NPs on laser hyperthermia efficacy, a thermal dose was considered as a practical parameter in thermotherapy regimes. From the time-temperature profiles of the cells, a CEM of 43 °C was calculated. The amounts of thermal doses applied to the cells on various treatments, including the sole action of laser and the combined action of laser and Fe_2O_3@Au or Fe_2O_3@Au-FA, are presented in the logarithmic scale in Figure 9. As shown in this figure, the presence of NPs inside the cells dramatically increased the thermal dose in a concentration-dependent manner. As expected from the temperature rise profiles of the cells, the targeted Fe_2O_3@Au-FA, coupled with laser irradiation, imparted a significantly higher thermal dose to the cells in comparison to non-targeted Fe_2O_3@Au. For example, while the cells without NPs received a negligible thermal dose of 0.0045 ± 0.00 min, this value was substantially enhanced to 3.79 ± 0.20 min for Fe_2O_3@Au NPs and 265.77 ± 8.27 min for Fe_2O_3@Au-FA at the same Au concentration of 40 μg/ml.

Cytotoxicity of Fe_2O_3@Au NPs

It is necessary to evaluate the cytotoxicity of the synthesized nanomaterials before further biomedical applications. Therefore, we tested the cytotoxicity of Fe_2O_3@Au NPs using MTT assay. The viability of KB cells incubated with different concentrations of Fe_2O_3@Au NPs is presented in Figure 10(a). It was found that Fe_2O_3@Au NPs induced more than 20% cell death at concentrations higher than 20 μg/ml. To make a comparison, the cytotoxicity of FA conjugated Fe_2O_3@Au NPs was also examined at the same concentration (20 μg/ml). As seen in Figure 10(b), there is no significant difference between the cytotoxicity of Fe_2O_3@Au-FA and Fe_2O_3@Au NPs. As a result, 20 μg/ml was selected as a suitable concentration for further studies and also for PTT of KB cells.

Results of flow cytometry studies

To determine the level of cell death and apoptosis induced in KB cells following PTT, we evaluated the *in vitro* effects of

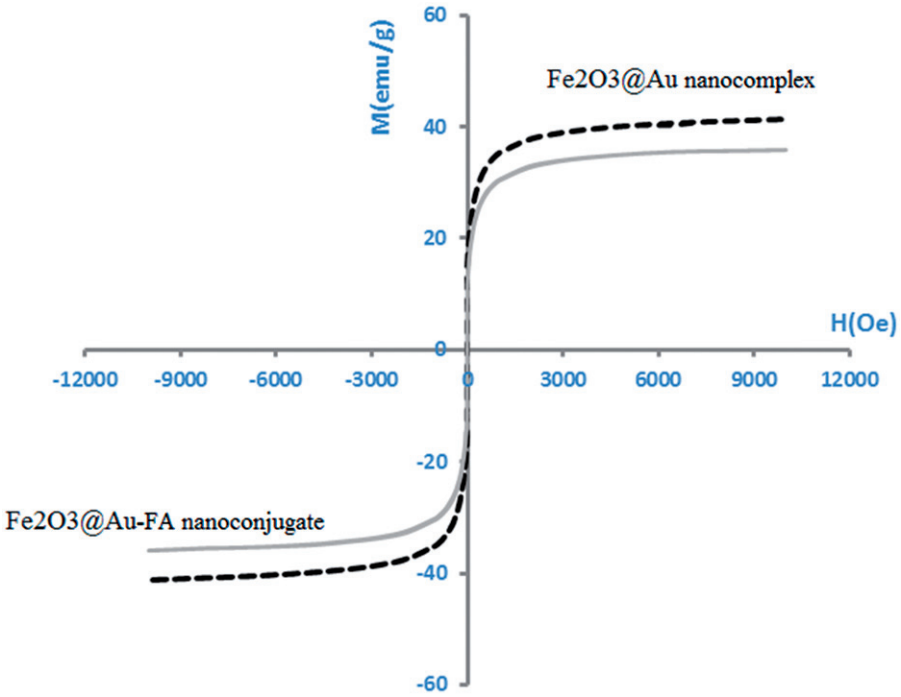

Figure 5. Magnetization curve of Fe_2O_3@Au nanocomplex and Fe_2O_3@Au-FA nanoconjugate.

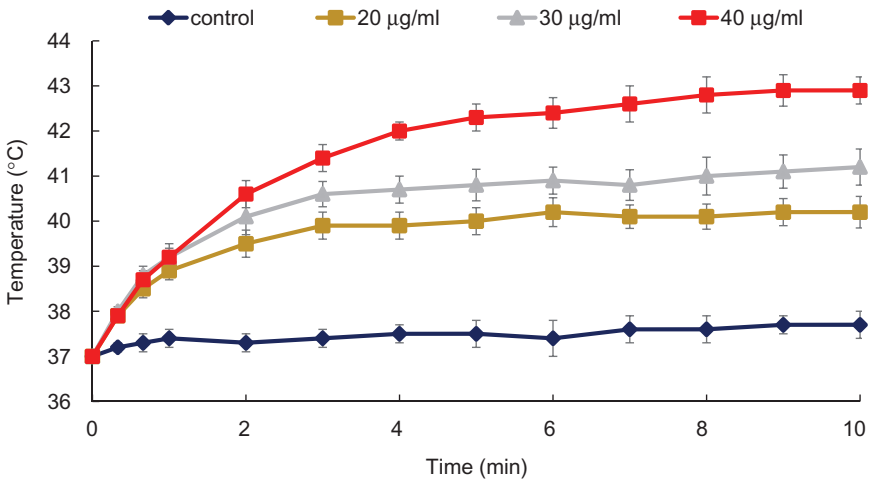

Figure 6. Temperature rise profile of the KB cancer cells incubated with Fe_2O_3@Au NPs at different Au concentrations upon administration of NIR laser (808 nm; 6 W/cm^2; 10 min).

both targeted and non-targeted NPs in the process of PTT by flow cytometry. As shown in Figure 11(a), laser or both types of NPs or laser alone did not highly increase the amount of cell death compared with the control group. Significant cell death was obtained when combination of laser and NPs was tested. In comparison with Fe_2O_3@Au NP, higher level of cell death was observed when Fe_2O_3@Au-FA nanoconjugate was used in the process of PTT. Moreover, the induction of apoptosis was increased when KB cells incubated with FA-targeted NPs were exposed by laser (Figure 11(b)).

Discussion

The increased temperature rise and the thermal dose due to the presence of Fe_2O_3@Au inside the cells upon NIR irradiation can be attributed to the gold plasmonic shell compartment of the NPs that possess the characteristic surface plasmon bands in the NIR region. Minimal absorption of light by the tissue in the NIR spectra provides a therapeutic window that allows for a deeper penetration of light inside the body. Unlike the spherical gold structures, the surface plasmon resonance (SPR) of the nanoshells are tuned to the NIR region. This is considered a great advantage for Fe_2O_3@Au core–shell nanoplatforms over spherical gold nanostructures as they are capable of converting NIR light to heat, thereby allowing for the treatment of deep-seated tumors [18]. When the gold plasmonic shell is subjected to light, the free electrons in the conduction band of AuNPs undergo a collective coherent oscillation. The amplitude of oscillation becomes maximum at a specific frequency of incident light; this is

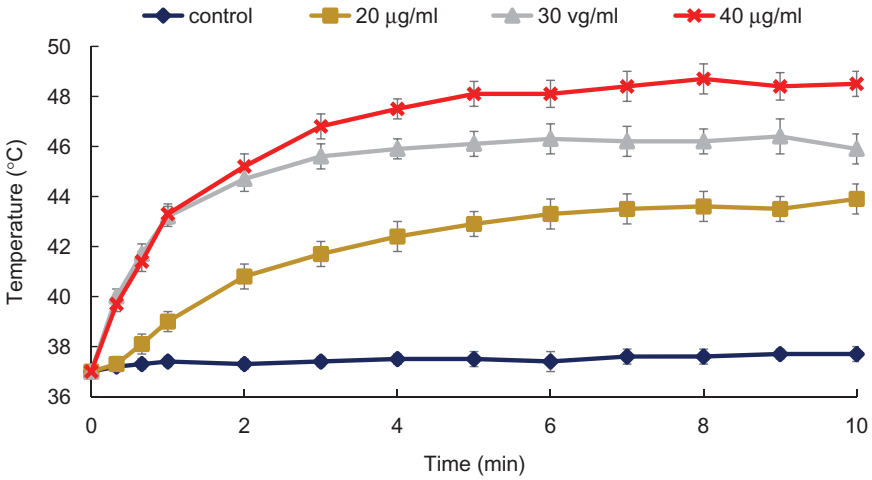

Figure 7. Temperature rise profile of the KB cancer cells incubated with FA conjugated Fe_2O_3@Au NPs at different Au concentrations upon administration of NIR laser (808 nm; 6 W/cm^2; 10 min).

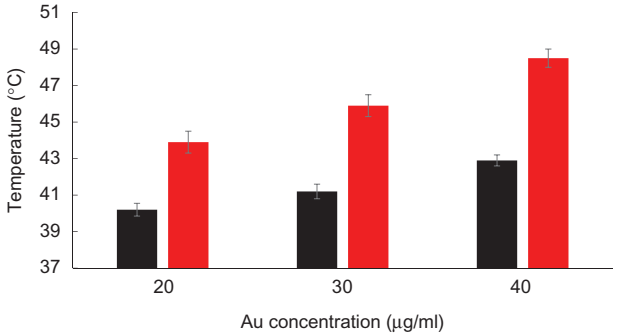

Figure 8. Final temperature rise of the KB cancer cells incubated with Fe_2O_3@Au (black) and Fe_2O_3@Au-FA NPs (red) at different Au concentration following 10 min NIR laser irradiation (808 nm; 6 W/cm^2).

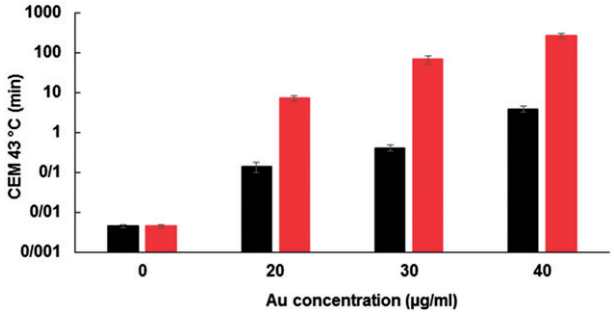

Figure 9. Thermal doses applied to the KB cancer cells for NIR laser irradiation (808 nm; 6 W/cm^2; 10 min) alone (concentration =0) and for combination of laser and Fe_2O_3@Au (black) and Fe_2O_3@Au-FA NPs (red) at different Au concentrations.

termed as surface plasmon resonance (SPR). The optical energy obtained by the oscillating electrons turns into heat and is transferred into the particle lattice via the electron–phonon relaxation. The heat diffuses away from the lattice via phonon–phonon relaxation, leading to an increased temperature of the surrounding medium [39,40].

Wang et al. [41] evaluated the photothermal efficiency of the gold magnetic NPs (GMNs) by monitoring the temperature rise of the GMNs solution under NIR laser irradiation (808 nm, 1 W/cm^2, 10 min). While water-free NPs showed an increased temperature of only 4.15 °C, the temperature of GMNs solution (50 μg/ml) increased by ~28 °C, demonstrating the efficient NIR absorption potential of gold magnetic core–-shell structures. This capability was then exploited to damage cancer cells, where the PTT of the HepG2 hepatocellular carcinoma cells in the presence of GMNs (100 μg/ml) caused an inhibition rate of 82.4%.

As shown in Figure 8, the cells exposed to FA-modified NPs reached higher temperature increases in comparison to non-FA modified NPs. Tables 1–3 present comparisons between the photothermal efficiency of Fe_2O_3@Au-FA and Fe_2O_3@Au NPs at different concentrations. Table 1 shows the temperature elevation rates for the KB cells loaded with various concentrations of Fe_2O_3@Au-FA and Fe_2O_3@Au NPs, following 10 min of NIR laser irradiation. Table 2 reports the 'X-fold' increase in the temperature elevation rate of the cells due to the presence of NPs, which is calculated using Equation (3):

$$\text{'X}-\text{fold' increase in temperature elevation rate} = \frac{\textit{Temperature elevation rate (with nanoparticles)}}{\textit{Temperature elevation rate (without nanoparticles)}} - 1 \quad (3)$$

Compared to the cells solely treated with the laser, the six-fold and 15.42-fold increase in the temperature elevation rate were obtained for the cells treated with laser plus Fe_2O_3@Au-FA and Fe_2O_3@Au NPs (40 μg/ml Au concentration), respectively. Table 3 also presents an increase in the peak temperature of KB cells treated by the NPs at the end of 10 min of the PTT operation in comparison to the cells without NPs.

FA is an ingredient required for cell proliferation and cancer cells supply this need through overexpression of the FA receptor on their surface [42,43]. The surface functionalization of Fe_2O_3@Au NPs with FA thus provides an active targeting strategy that directs the NPs towards the cell surface FA receptor, leading to enhanced uptake and efficient internalization of the NPs via receptor-mediated endocytosis [24,25].

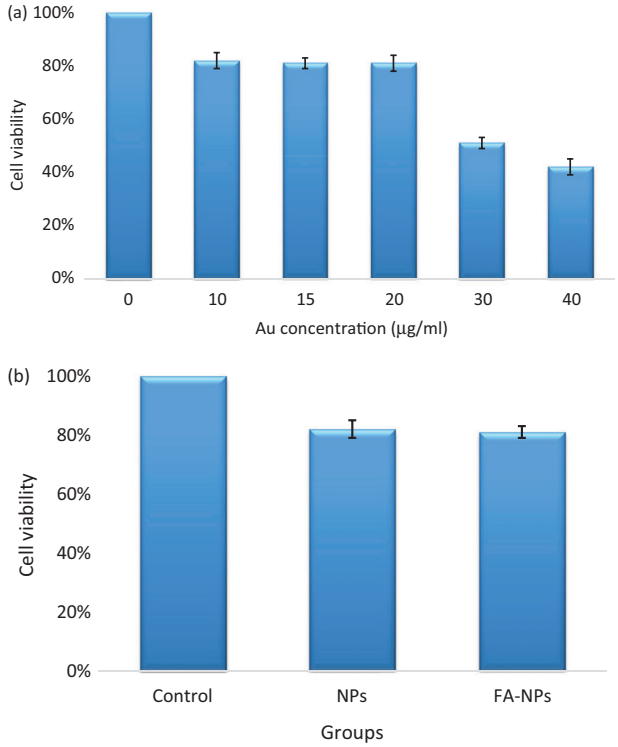

Figure 10. (a) The viability of KB cells incubated with different concentrations of nanoconjugates for 4 h. High level of cytotoxicity is observed for the concentrations greater than 20 μg/ml. (b) The viability of KB cells incubated with Fe_2O_3@Au (NPs) and Fe_2O_3@Au-FA (FA-NPs) for 4 h (concentration: 20 μg/ml).

Table 1. The temperature elevation rates of the KB cancer cells incubated with different concentrations of Fe_2O_3@Au NPs and Fe_2O_3@Au-FA NPs following NIR laser irradiation (808 nm; W/cm^2; 10 min).

	Au concentration			
Nanoparticles	0	20 μg/ml	30 μg/ml	40 μg/ml
Fe_2O_3@Au	0.07 °C/min	0.32 °C/min	0.42 °C/min	0.49 °C/min
Fe_2O_3@Au-FA	0.07 °C/min	0.69 °C/min	0.89 °C/min	1.15 °C/min

Table 2. The "X-fold" increases in temperature elevation rates of the KB cancer cells during laser irradiation in the presence of Fe_2O_3@Au NPs and Fe_2O_3@Au-FA NPs at different Au concentrations.

	Au concentration		
Nanoparticles	20 μg/ml	30 μg/ml	40 μg/ml
Fe_2O_3@Au	3.57×	5×	6×
Fe_2O_3@Au-FA	8.85×	11.71×	15.42×

For example, Gao et al. [44] evaluated the targeting efficiency of FA-conjugated silica-coated gold nanorods (FA-SiO_2@AuNR) towards the HepG2 hepatocellular carcinoma cells and reported a 2.65-fold higher cellular uptake rate for this nanocomplex in comparison to the non-FA conjugated nanocomplex. In another study, the facility of FA targeting was utilized for improving the PTT efficiency of the KB cancer cells. After laser irradiation, the survival of KB cells incubated with 20 μM AuNRs was reduced from 96.4 to 60.57%, whereas the FA-conjugated AuNRs at the same concentration further reduced the cell survival to 44.3% [45]. Accordingly, the higher temperature elevation rate of the KB cells incubated with Fe_2O_3@Au-FA NPs in comparison to those cells incubated with Fe_2O_3@Au NPs can be related to the enhanced accumulation of the targeted NPs inside the cells, providing more efficient PTT.

Table 3. The "X-fold" increase in peak temperature of the KB cancer cells incubated with Fe_2O_3@Au NPs and Fe_2O_3@Au-FA NPs at different Au concentrations with respect to 0% au concentration at the end of 10 min NIR laser irradiation.

	Au concentration		
Nanoparticles	20 μg/ml	30 μg/ml	40 μg/ml
Fe_2O_3@Au	1.06×	1.09×	1.13×
Fe_2O_3@Au-FA	1.16×	1.21×	1.28×

The positive impact of FA targeting on the promotion of PTT effectiveness would be more prominent if the temperature profile of the cells were analyzed from the perspective of the thermal dose. As shown in Figure 9, higher thermal doses were obtained for Fe_2O_3@Au-FA NPs in comparison to Fe_2O_3@Au NPs. For example, the obtained thermal dose in the presence of FA conjugated Fe_2O_3@Au NPs at a concentration of 20 μg/ml was found to be significantly higher than the thermal dose obtained with non-targeted Fe_2O_3@Au NPs even at a higher Au concentration of 40 μg/ml. Consequently, the exploitation of the FA targeting facility by enhancing the cellular uptake of NPs provides a unique opportunity to use lower NPs concentrations while achieving higher thermal doses, thereby offering improved laser hyperthermia efficiency. The data presented in Figure 11 also confirms that FA targeting improve the results of laser hyperthermia.

Conclusion

In this article, we reported the synthesis and characterization of Fe_2O_3@Au NPs with and without folate conjugation. The transient temperature rise of the cells loaded with Fe_2O_3@Au core-shell NPs was measured upon the administration of NIR laser. To normalize the different thermal histories,

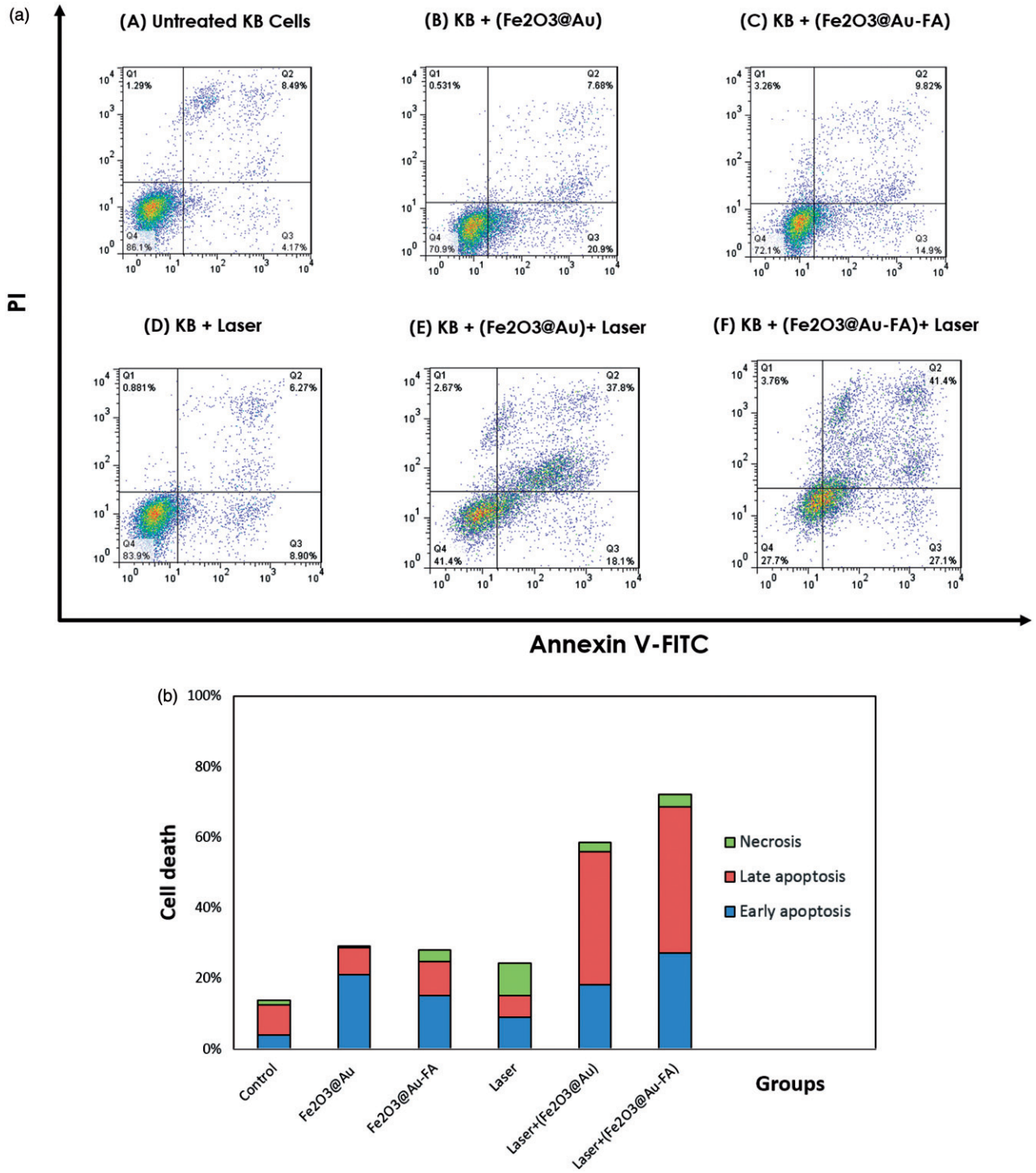

Figure 11. (a) Flow cytometric analysis to determine death modes of KB cells after receiving various treatments. (b) The percentage of necrotic and apoptotic KB cells after receiving various treatments.

the concept of thermal dose, which is relevant to the biological mechanisms involved in the hyperthermia regimes, was considered. The conjugation of FA with a high affinity for KB cancer cells appreciably caused the enhanced accumulation of the NPs inside the cells. Consequently, an obvious increase in the temperature elevation rate, subsequently applied thermal dose to the cells and apoptosis was attained when compared to the non-FA conjugated NPs. Therefore, the functionalization of NPs with FA provides a potential for improving laser hyperthermia efficiency through the reduction of the administrated concentration of NPs while achieving higher thermal doses and the power density of the laser used; furthermore, the time needed for a PTT operation could be potentially reduced.

Disclosure statement

No potential conflict of interest was reported by the authors.

ORCID

Ali Shakeri-Zadeh http://orcid.org/0000-0002-2847-9223

References

[1] Lin J, Chen X, Huang P. Graphene-based nanomaterials for bioimaging. Adv Drug Deliv Rev. 2016;105:242–254.

[2] Ryu JH, Lee S, Son S, et al. Theranostic nanoparticles for future personalized medicine. J Control Release. 2014;190:477–484.

[3] Kumar A, Zhang X, Liang XJ. Gold nanoparticles: emerging paradigm for targeted drug delivery system. Biotechnol Adv. 2013;31:593–606.

[4] Rana S, Bajaj A, Mout R, et al. Monolayer coated gold nanoparticles for delivery applications. Adv Drug Deliv Rev.2012; 64:200–216.

[5] Al Zaki A, Cormode D, Tsourkas A, et al. Increasing the therapeutic efficacy of radiotherapy using nanoparticles. In: Tofilon P, Camphausen K., editors. Increasing the therapeutic ratio of radiotherapy. Cancer drug discovery and development. Cham: Humana Press; 2017. p. 241–65.

[6] Her S, Jaffray DA, Allen C. Gold nanoparticles for applications in cancer radiotherapy: mechanisms and recent advancements. Adv Drug Deliv Rev. 2017;109:84–101.

[7] Shakeri-Zadeh A, Shiran M-B, Khoee S, et al. A new magnetic nanocapsule containing 5-fluorouracil: In vivo drug release, antitumor, and pro-apoptotic effects on CT26 cells allograft model. J Biomater Appl. 2014;29:548–556.

[8] Beik J, Abed Z, Ghoreishi FS, et al. Nanotechnology in hyperthermia cancer therapy: from fundamental principles to advanced applications. J Control Release. 2016;235:205–221.

[9] Beik J, Abed Z, Ghadimi-Daresajini A, et al. Measurements of nanoparticle-enhanced heating from 1MHz ultrasound in solution and in mice bearing CT26 colon tumors. J Therm Biol. 2016; 62:84–89.

[10] Huilgol NG, Gupta S, Sridhar CR. Hyperthermia with radiation in the treatment of locally advanced head and neck cancer: a report of randomized trial. J Cancer Res Ther. 2010;6:492–496.

[11] Colombo R, Da Pozzo LF, Salonia A, et al. Multicentric study comparing intravesical chemotherapy alone and with local microwave hyperthermia for prophylaxis of recurrence of superficial transitional cell carcinoma. J Clin Oncol. 2003;21:4270–4276.

[12] Daraee H, Eatemadi A, Abbasi E, et al. Application of gold nanoparticles in biomedical and drug delivery. Artif Cells Nanomed Biotechnol. 2016;44:410–422.

[13] Beik J, Abed Z, Shakeri-Zadeh A, et al. Evaluation of the sonosensitizing properties of nano-graphene oxide in comparison with iron oxide and gold nanoparticles. Physica E Low Dimens Syst Nanostruct. 2016;81:308–314.

[14] Dutz S, Hergt R. Magnetic particle hyperthermia-a promising tumour therapy? Nanotechnology. 2014;25:452001.

[15] Eustis S, El-Sayed MA. Why gold nanoparticles are more precious than pretty gold: noble metal surface plasmon resonance and its enhancement of the radiative and nonradiative properties of nanocrystals of different shapes. Chem Soc Rev. 2006;35:209–217.

[16] Neshastehriz A, Tabei M, Maleki S, et al. Photothermal therapy using folate conjugated gold nanoparticles enhances the effects of 6MV X-ray on mouth epidermal carcinoma cells. J Photochem Photobiol. 2017;172:52–60.

[17] Yang X, Yang M, Pang B, et al. Gold nanomaterials at work in biomedicine. Chem Rev. 2015;115:10410–10488.

[18] Qin Z, Bischof JC. Thermophysical and biological responses of gold nanoparticle laser heating. Chem Soc Rev. 2012;41: 1191–1217.

[19] Shakeri-Zadeh A, Kamrava SK, Farhadi M, et al. A scientific paradigm for targeted nanophotothermolysis; the potential for nanosurgery of cancer. Lasers Med Sci. 2014;29:847–853.

[20] Tripathi R, Shrivastav A, Shrivastav B. Biogenic gold nanoparticles: as a potential candidate for brain tumor directed drug delivery. Artif Cells Nanomed Biotechnol. 2015;43:311–317.

[21] Li Y, Lin J, Yang X, et al. Self-assembled nanoparticles based on amphiphilic anticancer drug–phospholipid complex for targeted drug delivery and intracellular dual-controlled release. ACS Appl Mater Interfaces. 2015;7:17573–17581.

[22] Li Y, Lin J, Wu H, et al. Orthogonally functionalized nanoscale micelles for active targeted codelivery of methotrexate and mitomycin C with synergistic anticancer effect. Mol Pharmaceutics. 2015;12:769–782.

[23] Li Y, Lin J, Huang Y, et al. Self-targeted, shape-assisted, and controlled-release self-delivery nanodrug for synergistic targeting/ anticancer effect of cytoplasm and nucleus of cancer cells. ACS Appl Mater Interfaces. 2015;7:25553–25559.

[24] Samadian H, Hosseini-Nami S, Kamrava SK, et al. Folate-conjugated gold nanoparticle as a new nanoplatform for targeted cancer therapy. J Cancer Res Clin Oncol. 2016;142:2217–2229.

[25] Mansoori GA, Brandenburg KS, Shakeri-Zadeh A. Cancer nanotechnology treatment through folate conjugated gold, nanoparticles. Proceedings of WCC. 2010;2:1911.

[26] Mansoori GA, Brandenburg KS, Shakeri-Zadeh A. A comparative study of two folate-conjugated gold nanoparticles for cancer nanotechnology applications. Cancers. 2010;2:1911–1928.

[27] Beik J, Jafariyan M, Montazerabadi A, et al. The benefits of folic acid-modified gold nanoparticles in CT-based molecular imaging: radiation dose reduction and image contrast enhancement. Artif Cells Nanomed Biotechnol. 2009. DOI:10.1080/21691401.2017.1408019

[28] Hu Y, Wang R, Wang S, et al. Multifunctional Fe_3O_4@ Au core/shell nanostars: a unique platform for multimode imaging and photothermal therapy of tumors. Sci Rep. 2016;6:28325.

[29] Kang YS, Risbud S, Rabolt JF, et al. Synthesis and characterization of nanometer-size Fe_3O_4 and γ-Fe_2O_3 particles. Chem Mater. 1996;8:2209–2211.

[30] Lyon JL, Fleming DA, Stone MB, et al. Synthesis of Fe oxide core/Au shell nanoparticles by iterative hydroxylamine seeding. Nano Lett. 2004;4:719–723.

[31] Van Steenis J, Van Maarseveen E, Verbaan F, et al. Preparation and characterization of folate-targeted pEG-coated pDMAEMA-based polyplexes. J Control Release. 2003;87:(1):167–76.

[32] Chan P, Kurisawa M, Chung JE, et al. Synthesis and characterization of chitosan-g-poly (ethylene glycol)-folate as a non-viral carrier for tumor-targeted gene delivery. Biomaterials. 2007;28: 540–549.

[33] Gao J, Huang X, Liu H, et al. Colloidal stability of gold nanoparticles modified with thiol compounds: bioconjugation and application in cancer cell imaging. Langmuir. 2012;28:4464–4471.

[34] Sapareto SA. The biology of hyperthermia in vitro. In: Nussbaum GH, editor. Physical aspects of hyperthermia. New York (NY): American Institute of Physics; 1982. p. 1–19.

[35] Sapareto SA, Hopwood LE, Dewey WC, et al. Effects of hyperthermia on survival and progression of Chinese hamster ovary cells. Cancer Res. 1978;38:393–400.

[36] Lynch TJ, Bell DW, Sordella R, et al. Activating mutations in the epidermal growth factor receptor underlying responsiveness of non-small-cell lung cancer to gefitinib. N Engl J Med. 2004;350:2129–2139.

[37] Sardar R, Funston AM, Mulvaney P, et al. Gold nanoparticles: past, present, and future. Langmuir. 2009;25:13840–13851.

[38] Zhang J, Rana S, Srivastava R, et al. On the chemical synthesis and drug delivery response of folate receptor-activated, polyethylene glycol-functionalized magnetite nanoparticles. Acta Biomaterialia. 2008;4:40–48.

[39] Huang X, El-Sayed MA. Gold nanoparticles: optical properties and implementations in cancer diagnosis and photothermal therapy. Int J Adv Res. 2010;1:13–28.

[40] Govorov AO, Richardson HH. Generating heat with metal nanoparticles. Nano Today. 2007;2:30–38.

[41] Wang X, Liu H, Chen D, et al. Multifunctional Fe_3O_4@ P (St/MAA)@ Chitosan@ Au core/shell nanoparticles for dual imaging and photothermal therapy. ACS Appl Mater Interfaces. 2013;5:4966–4971.

[42] Ghaznavi H, Hosseini-Nami S, Kamrava SK, et al. Folic acid conjugated PEG coated gold-iron oxide core-shell nanocomplex as a potential agent for targeted photothermal therapy of cancer. Artif Cells Nanomed Biotechnol. 2017. DOI:10.1080/21691401.2017.1384384

[43] Chiani M, Norouzian D, Shokrgozar MA, et al. Folic acid conjugated nanoliposomes as promising carriers for targeted delivery of bleomycin. Artif Cells Nanomed Biotechnol. 2017. DOI:10.1080/21691401.2017.1337029

[44] Gao B, Shen L, He KW, et al. GNRs@ SiO2-FA in combination with radiotherapy induces the apoptosis of HepG2 cells by modulating the expression of apoptosis-related proteins. Int J Mol Med. 2015;36:1282–1290.

[45] Mehdizadeh A, Pandesh S, Shakeri-Zadeh A, et al. The effects of folate-conjugated gold nanorods in combination with plasmonic photothermal therapy on mouth epidermal carcinoma cells. Lasers Med Sci. 2014;29:939–948.